

Laboratory 3: Projectile motion under the action of air resistance

Jordan Ahern 21363697

November 13, 2022

1 INTRODUCTION

Projectile motion is a commonly encountered problem. This problem can be solved analytically, and relatively simply, when air resistance is not considered. In the physical world this is often not a good approximation. This report investigated the motion of projectiles where air resistance was non-negligible. The addition of the restive force to the equations of projectile makes analytical solutions much more difficult to solve analytically. Instead, methods were implemented in Python to numerically solve the equations of a projectile under air resistance. These methods were used to investigate three main areas, the relationships between velocity and air resistance, the effects of air resistance on vertical motion, the trajectories of particles under resistance. In these sections the relationship between resistance and velocity was seen to be both linear and quadratic, with one of these terms being negligible depending on the initial conditions of a particular particle. It was observed that air resistance can impose a "terminal velocity" on a falling object, increasing the time it takes a falling particle to hit the ground. All forms of air resistance decreased the range of projectiles. The optimal launch angle for a particle, always 45° without air resistance, was noted to be dependent on the projectiles initial conditions when resistance was included. Theses trials were completed in Python 3, with the Numpy and Matplotlib libraries within the Anaconda Spyder environment.

2 METHODOLOGY

The equations of motion of projectiles were altered to include air resistance by the addition of a new force term to Newton's 2nd law. This term is velocity dependent and acts against the direction of velocity, $\mathbf{F} = -f(V)\hat{\mathbf{u}}$. This function is well approximated by

$$f(V) = bV + cV^2 \quad (2.1)$$

with $b = B D$ and $c = C D^2$. Here, D was the cross-sectional diameter of the projectile, $B = 1.6 \cdot 10^{-4} \text{ N s m}^{-2}$, and $C = 0.25 \text{ N s}^2 \text{ m}^{-4}$.

2.1 EXERCISE 1: AIR RESISTANCE AND PARTICLE CONDITIONS

While, Equation 2.1 was a good approximation for air resistance it was rather difficult to work with in terms of finding the equations of motion. Since, this expression was a linear combination of linear and quadratic terms it was predictable that under certain conditions one of the terms would become neglectable. This section plotted the quantities of bV and cV^2 against the conditions of diameter and velocity, $D \times V$, to give predictions for ranges within which air resistance can be simplified.

These ranges were then used to categorise the which term, if either, in Equation 2.1, could be ignored when discussing a number of different projectiles; a baseball, a tiny drop of oil, and a raindrop.

2.2 EXERCISE 2: VERTICAL MOTION UNDER LINEAR AIR RESISTANCE

This exercise examined the vertical motion of a spherical grain of dust with a mass density of $\rho = 2 \times 10^3 \text{ kg m}^{-3}$ and diameter $D = 10^{-4} \text{ m}$. Taking $M = \rho \cdot \frac{4}{3}\pi \left(\frac{D}{2}\right)^3$ the mass of this grain was found, $M = 1.05 \cdot 10^{-9} \text{ kg}$. The maximum velocity of this particle was taken to be the velocity where drag equaled weight

$$Mg = bV_T \quad (2.2)$$

with g being gravitational acceleration.

The air resistance on this grain of dust was approximated to be linear only for the remainder of this exercise. The vertical velocity, starting from rest, of this particle was solved numerically and plotted against time. This numerical solution repeatedly iterated the current vertical velocity by

$$\Delta V_y = -g\Delta t - \frac{b}{M}V_y\Delta t \quad (2.3)$$

The plot was used to check the numerical solution for terminal velocity against the analytical solution, Equation 2.2. For the case of an exclusively linear drag force the velocity of a projectile is analytically solvable by

$$V_y(t) = \frac{Mg}{b} \left(\exp\left(-\frac{bt}{M}\right) - 1 \right) \quad (2.4)$$

This analytical solution was used to test the accuracy of the numerical solution over time. The numerical method was then adapted

$$\Delta Y = V_y \Delta t \quad (2.5)$$

to solve for the vertical position of the particle. The time a particle took to reach the ground, when dropped from a particular height, was plotted against the mass of the particle.

2.3 EXERCISE 3: TRAJECTORY UNDER LINEAR AIR RESISTANCE

Similarly to Equation 2.3, the horizontal velocity of a projectile was found through iterating the instantaneous horizontal velocity by

$$\Delta V_x = -\frac{b}{M} V_x \Delta t \quad (2.6)$$

Analogously to Equation 2.5, this expression could numerically calculate the change in horizontal position over time. The trajectory was then found by plotting Y against X. The trajectory of a particle under varying strengths of air resistance was plotted against the ideal case of no air resistance.

The functions were then altered to take in initial velocity in polar forms

$$V_x = V \cos \theta \quad (2.7) \qquad V_y = V \sin \theta \quad (2.8)$$

to test how the launch angle effects the range of a projectile. The range of a projectile under linear resistance was plotted against the launch angle for different dampening constants. The optimal angle, the one with the largest range, was plotted against the mass of the projectile.

2.4 EXERCISE 4: TRAJECTORY UNDER QUADRATIC AIR RESISTANCE

For the case of quadratic air resistance there was no analytical solution to find and only numerical methods were used. Recalling Equations 2.3 and 2.6, the new equations of motion were now coupled according to

$$\Delta V_x = -\frac{c}{M} \cdot \sqrt{V_x^2 + V_y^2} \cdot V_x \Delta t \quad (2.9) \quad \Delta V_y = -g \Delta t - \frac{c}{M} \cdot \sqrt{V_x^2 + V_y^2} \cdot V_y \Delta t \quad (2.10)$$

The trajectories of particles under both cases of air resistance, and no resistance were then plotted together.

3 RESULTS

3.1 EXERCISE 1: AIR RESISTANCE AND PARTICLE CONDITIONS

In the following graphs the individual components share the left y-axis and the sum of components to the right.

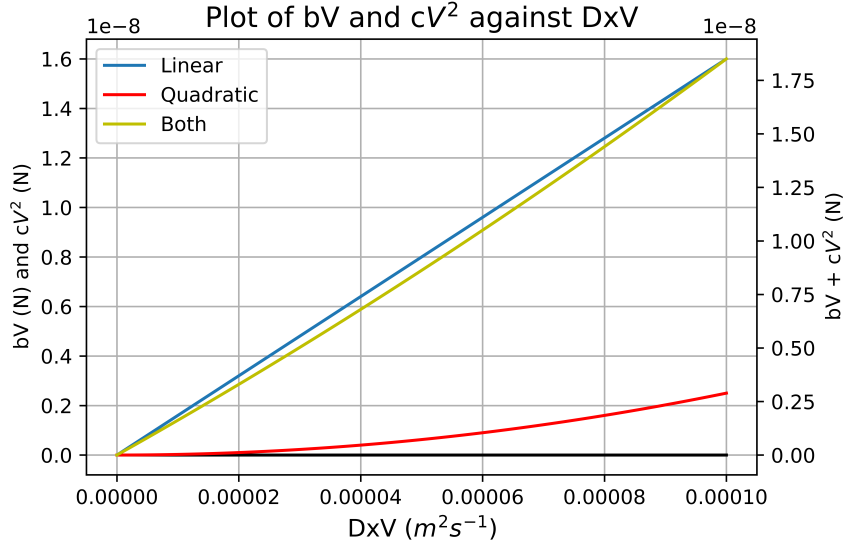


Figure 3.1: Graph of bV , cV^2 , and $f(V)$ against DxV up to 10^{-4} .

In Figure 3.1, the quadratic term was seen to be close to zero up until the region of $D \times V \approx 4 \cdot 10^{-5}$. Up to the order of 10^{-4} the combination of both terms closely tracked the linear term. At the final point, just over 10% of the magnitude of “Both” is due to the quadratic term so it can be said to be approaching relevance from there on.

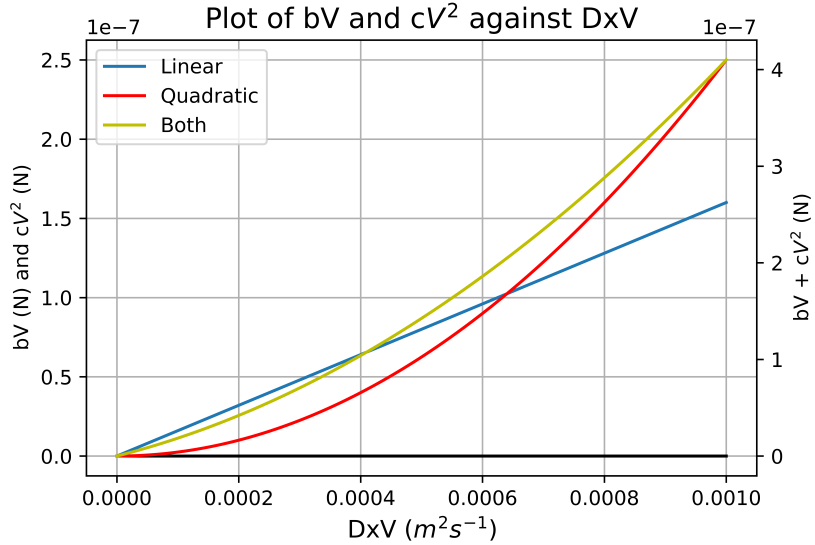


Figure 3.2: Graph of bV , cV^2 , and $f(V)$ against DxV up to 10^{-3} .

The graph in Figure 3.2, both terms clearly had an affect on the magnitude of resistance. The “Both” line began to curve but not to the same degree as the purely quadratic line. Just passed $D \times V \approx 6 \cdot 10^{-4}$ the two lines meet and both terms contribute roughly equal magnitudes to the total. Before this point linear was the greater contribution, after this point quadratic will be larger, but linear will still be relevant for some interval.

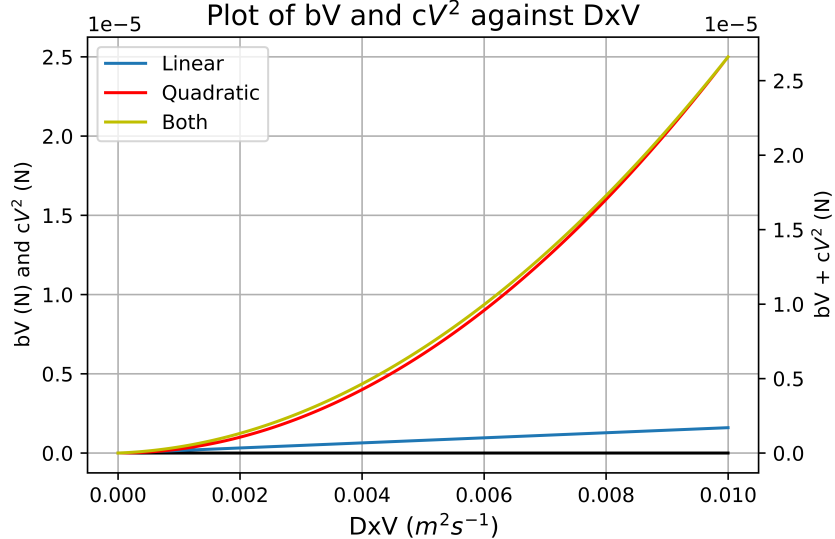


Figure 3.3: Graph of bV , cV^2 , and $f(V)$ against DxV up to 10^{-2} .

Figure 3.3 demonstrated that the quadratic term began to take over the total magnitude of air resistance. On the latter end of the graph the “Linear” and “Both” curves began to converge. At $D \times V 10^{-2}$ the linear term had already begun to contribute less than 10% of the total magnitude.

Based on the above graphs, the intervals

$$0 < D \times V < 10^{-4} \Rightarrow f(V) \approx bV \quad (3.1)$$

$$10^{-4} < D \times V < 10^{-2} \Rightarrow f(V) = bV + cV^2 \quad (3.2)$$

$$10^{-2} < D \times V \Rightarrow f(V) \approx cV^2 \quad (3.3)$$

can roughly describe the conditions for which either the quadratic or linear term, or neither, can be neglected. These intervals assist in the categorisation of the resistive force acting on specific projectiles.

	Baseball	Oil Drop	Rain Drop
Diameter (m)	$7 \cdot 10^{-2}$	$1.5 \cdot 10^{-6}$	$1 \cdot 10^{-3}$
Speed (m s^{-1})	5	$5 \cdot 10^{-5}$	1
$D \times V (\text{m}^2 \text{s}^{-1})$	0.35	$7.5 \cdot 10^{-11}$	$1 \cdot 10^{-3}$
$f(V)$ State	bV	cV^2	$bV + cV^2$

Table 3.1: Table for classification of air resistance.

These results are in line with similar predictions made in textbooks [1].

3.2 EXERCISE 2: VERTICAL MOTION UNDER LINEAR AIR RESISTANCE

This relationship, Equation 2.2 gave the terminal velocity, the maximum downwards velocity in free-fall, to be $V_T \approx 0.643 \text{ m s}^{-1}$. This gave $D \times V 10^{-5}$ for the given spherical grain of dust. According to Figure 3.1 this region is mostly linear and the value is within the Interval 3.1 which was defined to give $f(V) \approx bV$, therefore a linear air resistance is a good approximation for this projectile.

Unless stated, this section used $b = 16 \cdot 10^{-9} \text{ N s m}^{-1}$, $M = 1.05 \cdot 10^{-9} \text{ kg}$, and $\Delta t = 0.001$.

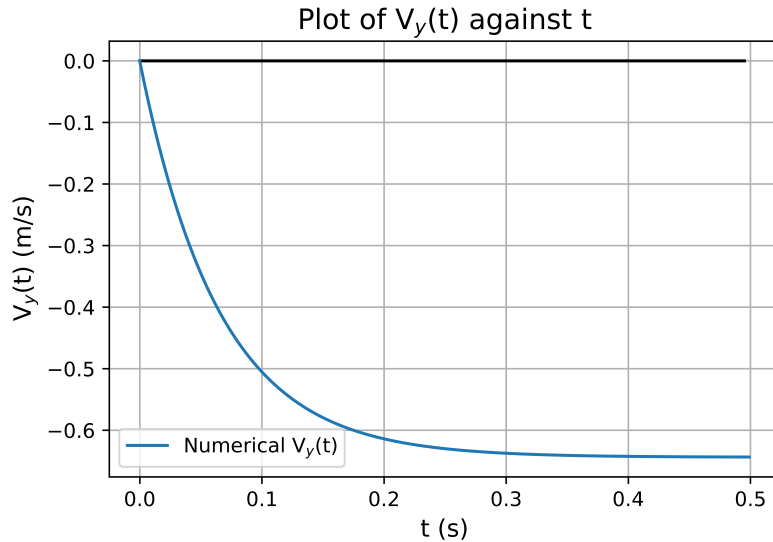


Figure 3.4: Graph of vertical velocity, over 0.5 s, starting from rest.

In Figure 3.4, velocity is negative as the particle is falling. The projectile was seen to start with a large acceleration which gradually levels off with time. The velocity was observed to be approaching the magnitude of 0.643 m s^{-1} , which matches the analytical calculation for terminal velocity, the final value was confirmed by printing the list that was graphed. This supported the numerical calculation.

This graph was repeated for much larger masses, up to 10^{-4} before computation time was a serious issue, the same curve was seen to form but for a larger terminal velocity and in a longer time. These results were in line with Equation 2.2, which showed the terminal velocity to be proportional to the objects mass.

Figure 3.5 described a right-skewed distribution for the error in the numerical method over time. The error peaked quickly and early in the motion, this was the region in which the projectile had the largest acceleration which would be most liable to be incorrectly modeled by the larger time jumps made by the numerical method over infinitesimals used in integrating the analytical solution. As time increased and the acceleration approached zero the numerical solution corrected itself and the error also approached zero. The accuracy of the numerical method potentially more accurate over longer time periods. As previously mentioned, much of the error was also due to they size of the time jumps,

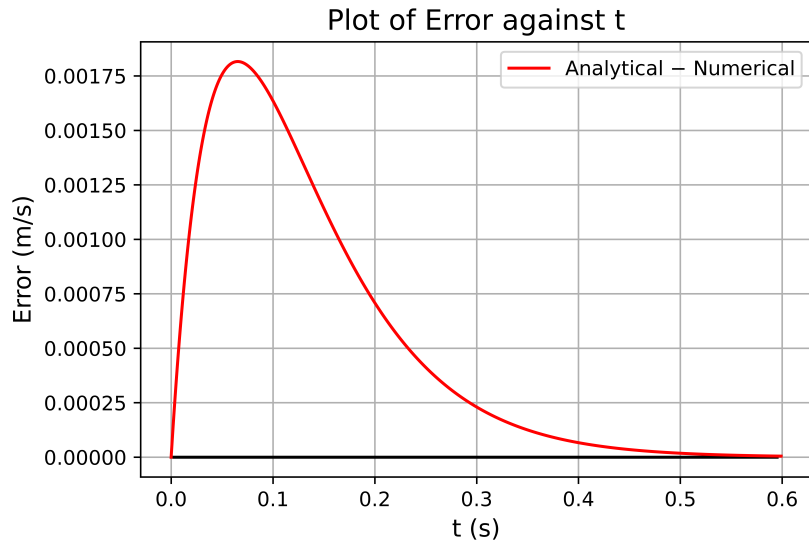


Figure 3.5: Graph of the error between the analytical and numerical solutions for vertical velocity over 0.6 s, $\Delta t = 0.001$.

accuracy would be improved as these time intervals, Δt , were made shorter.

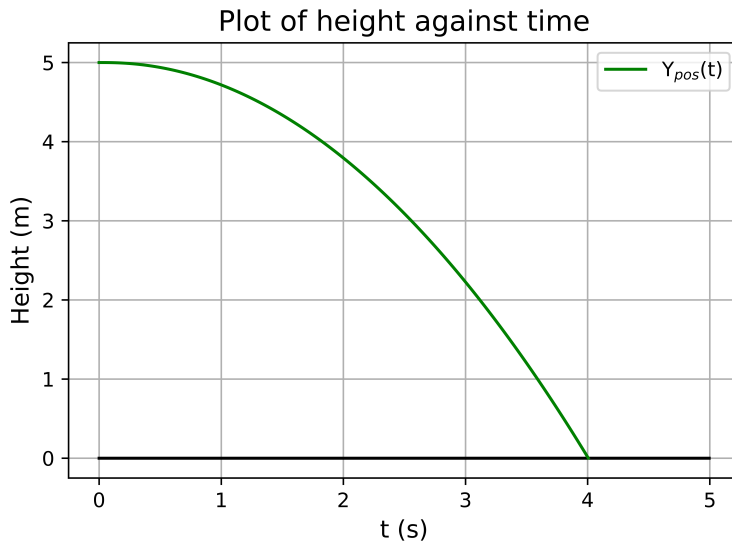


Figure 3.6: Graph of time for dust to reach the ground when dropped from rest at 5 m.

The trajectory seen in Figure 3.6 appeared to begin parabolic but the arc smooth out as time went on, being consistent with the particle reaching a terminal velocity. It was clear from Figure 3.7, that a heavier object will hit the ground sooner than a lighter one. This does not mean the objects are accelerating at different rates, g does not depend on object mass, instead larger masses have larger terminal velocities, according to Equation 2.2. Over very tiny distances the mass would possibly have little effect on

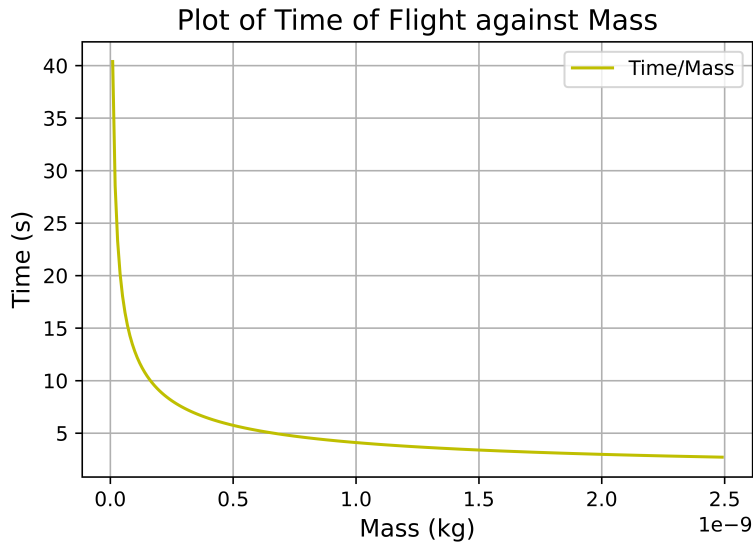


Figure 3.7: Graph of the time to strike ground from a 5 m drop from rest for a range of masses from $1 \cdot 10^{-11}$ kg to $2.5 \cdot 10^{-9}$ kg.

the time to reach the ground. Additionally, very low, zero, dampening constants would reduce, remove, the mass dependence.

3.3 EXERCISE 3: TRAJECTORY UNDER LINEAR AIR RESISTANCE

Unless stated, this section used $M = 1.05 \cdot 10^{-9}$ kg and $\Delta t = 0.001$.

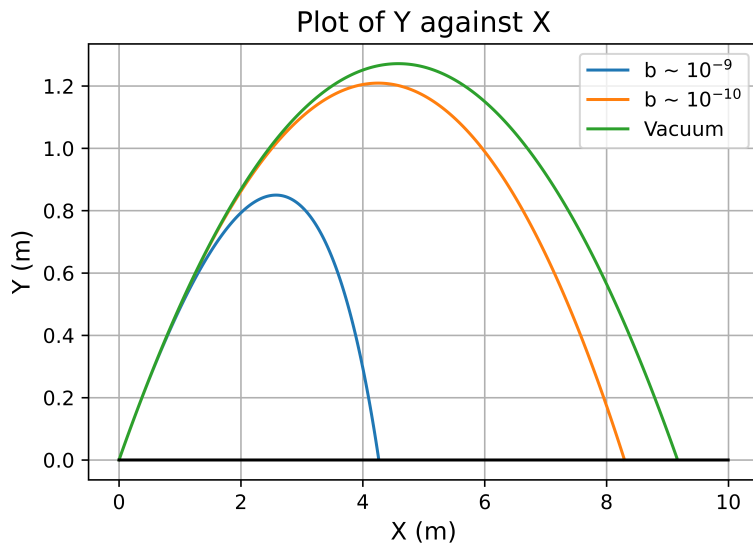


Figure 3.8: Graph of projectile trajectories for initial velocities $V_x = 9 \text{ m s}^{-1}$ and $V_y = 5 \text{ m s}^{-1}$ and labelled dampening constants. Vacuum: $b = 0$.

Air resistance was noted to noticeably effect the projectile trajectory in Figure 3.8. Where there was no resistance a symmetrical parabolic curve was followed but this symmetry was broken by any amount of non-conservative air resistance. Air drag also reduced both maximum altitude and range of the projectile.

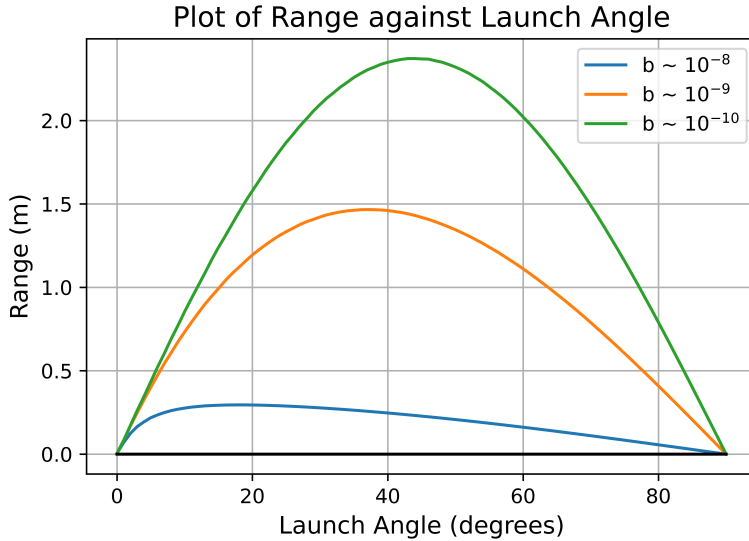


Figure 3.9: Graph of projectile ranges against launch angles for a range of drag constants and for initial velocity = 5 m s⁻¹.

It was demonstrated, by Figure 3.9, that as the resistance constant became larger, the optimal launch angle became smaller than the case of zero drag (45°).

Larger masses were seen to have larger optimal launch angles, Figure 3.10, which correlates with larger masses reducing the effects of air drag. The trend appeared to be potentially approaching 45°. This curve was not smooth, and made some very sudden oscillations in places. One possible part of this is that only whole numbered degrees were considered to conserve computing resources. Potentially, a larger explanation is that certain trajectories may have gone below the x-axis due to the relatively large numerical steps, $\Delta t = 0.001$, this could have made the occasional less optimal angle appear to give slightly larger ranges. A simplistic fix would be to decrease the step size but this would multiply the already highly inefficient computation time. It could be more efficient to implement a more advance numerical method such as Runge-Kutta to improve accuracy as zero is approached.

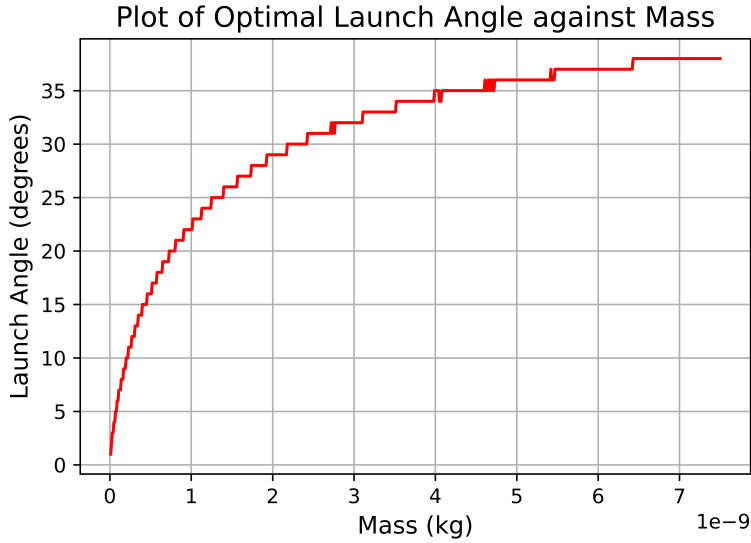


Figure 3.10: Graph of the optimal launch angle for projectiles with dampening constant $b = 16 \cdot 10^{-9} \text{ N s m}^{-1}$, initial velocity = 29 m s^{-1} , and with masses from $1 \cdot 10^{-11} \text{ kg}$ to $7.5 \cdot 10^{-9} \text{ kg}$.

3.4 EXERCISE 4: TRAJECTORY UNDER QUADRATIC AIR RESISTANCE

This section used $b = 1.6 \cdot 10^{-9} \text{ N s m}^{-1}$, $c = 2.5 \cdot 10^{-9} \text{ N s}^2 \text{ m}^{-2}$ and $\Delta t = 0.001$.

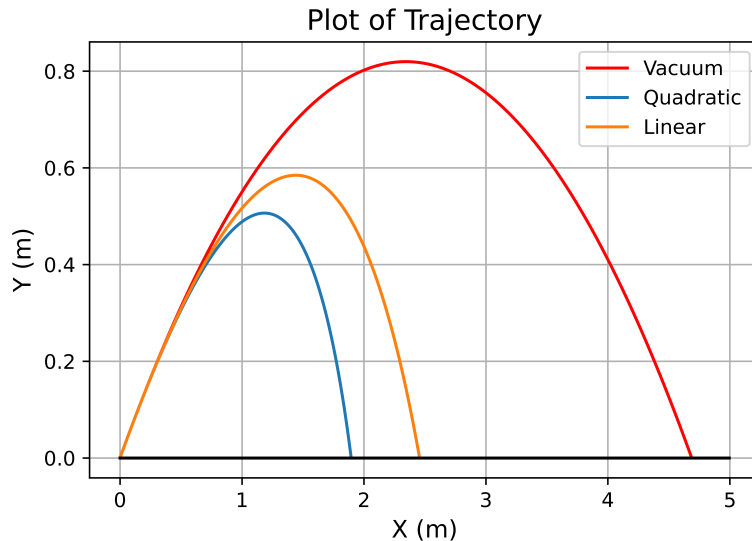


Figure 3.11: Graph of the trajectories of particles under different forms of dampening constant. With initial velocity = 7 m s^{-1} , launch angle = 35° and with mass = $1.05 \cdot 10^{-9} \text{ kg}$.

Plotting trajectories for all three cases clearly showed, Figure 3.11, that quadratic resistance also breaks the symmetry of motion, as it would be expected to.

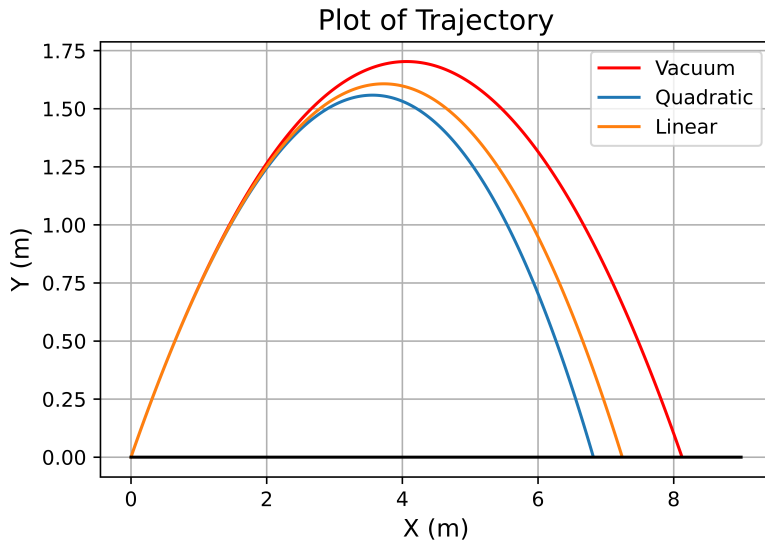


Figure 3.12: Graph of the trajectories of particles under different forms of dampening constant. With initial velocity = 9 m s^{-1} , launch angle = 40° and with mass = $1.05 \cdot 10^{-8} \text{ kg}$.

It was again seen, in Figure 3.12, that larger masses reduce the influences of air resistance, seen by how all three arcs are relatively close compared to when mass is an order of magnitude smaller.

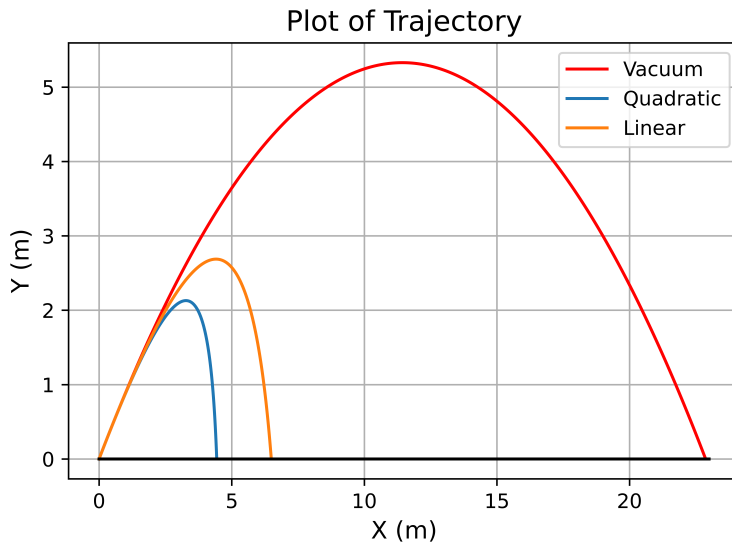


Figure 3.13: Graph of the trajectories of particles under different forms of dampening constant. With initial velocity = 15 m s^{-1} , launch angle = 43° and with mass = $1.05 \cdot 10^{-9} \text{ kg}$.

As expected velocity is a clear force multiplier for both forms of air resistance, Figure

3.13. The no resistance case had 4-5 times the range of both other cases as a result of the larger initial velocity than in the previous two figure.

4 CONCLUSION

This report successfully demonstrated the usage of numerical simulations to solve for the motion of projectiles in real world environments, including air resistance. Numerical calculations came to the same conclusions as two the form of air drag experienced by particular particles as in the literature [1]. Where a numerical solution could be found such as for terminal velocity and vertical velocity under linear resistance, Equations 2.2 and 2.4, the numerical results were in-line with the analytical values, Figures 3.4 and 3.5. Numerical methods were both able to plot sensible projectile trajectories but were also able to solve problems made complicated by air resistance. Two such problems being the time of flight of a particle under air resistance and the optimal launch angles of a particular projectile with air resistance, Figures 3.6 and 3.9. While most exercises were concerned with linear drag only, the implementation of quadratic drag in Section 3.4 could be easily repeated for the previous sections where that required; say a footballs optimal launch angle were being found rather than a spherical grain of dust.

5 BIBLIOGRAPHY

REFERENCES

¹J. R. Taylor, “Chapter 2 projectiles and charged particles”, in *Classical mechanics* (University Science Books, 2005), pp. 45–46.

LIST OF TABLES

3.1	Table for classification of air resistance.	5
-----	---	---

LIST OF FIGURES

3.1	Graph of bV , cV^2 , and $f(V)$ against DxV up to 10^{-4}	4
3.2	Graph of bV , cV^2 , and $f(V)$ against DxV up to 10^{-3}	4
3.3	Graph of bV , cV^2 , and $f(V)$ against DxV up to 10^{-2}	5
3.4	Graph of vertical velocity, over 0.5 s, starting from rest.	6
3.5	Graph of the error between the analytical and numerical solutions for vertical velocity over 0.6 s, $\Delta t = 0.001$	7
3.6	Graph of time for dust to reach the ground when dropped from rest at 5 m.	7
3.7	Graph of the time to strike ground from a 5 m drop from rest for a range of masses from $1 \cdot 10^{-11}$ kg to $2.5 \cdot 10^{-9}$ kg.	8

3.8	Graph of projectile trajectories for initial velocities $V_x = 9 \text{ m s}^{-1}$ and $V_y = 5 \text{ m s}^{-1}$ and labelled dampening constants. Vacuum: $b = 0$	8
3.9	Graph of projectile ranges against launch angles for a range of drag constants and for initial velocity = 5 m s^{-1}	9
3.10	Graph of the optimal launch angle for projectiles with dampening constant $b = 16 \cdot 10^{-9} \text{ N s m}^{-1}$, initial velocity = 29 m s^{-1} , and with masses from $1 \cdot 10^{-11} \text{ kg}$ to $7.5 \cdot 10^{-9} \text{ kg}$	10
3.11	Graph of the trajectories of particles under different forms of dampening constant. With initial velocity = 7 m s^{-1} , launch angle = 35° and with mass = $1.05 \cdot 10^{-9} \text{ kg}$	10
3.12	Graph of the trajectories of particles under different forms of dampening constant. With initial velocity = 9 m s^{-1} , launch angle = 40° and with mass = $1.05 \cdot 10^{-8} \text{ kg}$	11
3.13	Graph of the trajectories of particles under different forms of dampening constant. With initial velocity = 15 m s^{-1} , launch angle = 43° and with mass = $1.05 \cdot 10^{-9} \text{ kg}$	11